Mechanics Research Communications 155 (2026) 104702

Contents lists available at ScienceDirect

Mechanics Research Communications

journal homepage: www.elsevier.com/locate/mechrescom

Stiffness and buckling behavior of woven columns

Jaimie Krankel [a], Guowei Wayne Tu [b], Evgueni T. Filipov [a,b,*]

[a] Deployable and Reconfigurable Structures Laboratory, Department of Mechanical Engineering, University of Michigan, Ann Arbor, MI, USA
[b] Deployable and Reconfigurable Structures Laboratory, Department of Civil and Environmental Engineering, University of Michigan, Ann Arbor, MI, USA

ARTICLE INFO

Keywords:
Woven structure
Analytical model
Shell buckling
Local buckling

ABSTRACT

Woven shell structures are beneficial for applications requiring lightweight, damage resilience, and design tunability, such as in wearable devices, soft robotics, and aerospace systems. A fundamental component of woven structures is the woven column. While the mechanical properties of a woven column can be determined using sophisticated finite element (FE) simulations, these FE models are computationally expensive and do not explain the underlying mechanics behind scaling relationships. In this work, we derive purely analytical models for the buckling load and stiffness of woven columns, and discuss the criteria that lead to different buckling modes of the woven columns. The simulated results based on our models closely match experimental data across various weave design parameters. This work advances our understanding of the mechanics of woven systems and serves as a baseline for the design of next-generation hierarchical structures and materials.

1. Introduction

The long-standing craft of weaving has gained traction in modern engineering due to its mechanical strength, damage tolerance, and lightweight properties. These intrinsic benefits of weaving make it suitable for smart material devices, soft robotics, aerospace applications, and more [1–5]. The plain weave (Fig. 1a), in which perpendicular weavers alternate over and under each other, is the most commonly implemented pattern. This simple weave pattern achieves tight interlocking of material, making for strong and durable structures [6]. Previous work shows that plain woven 3D shell structures have much greater resilience [1] yet they share similar stiffness to their continuous counterparts, as demonstrated in Fig. 1b.

Similar to the continuous cylindrical shell, the woven column is a fundamental unit of 3D woven shell structures. Cylindrical shell buckling has been widely studied, and there exist closed-form solutions for their behaviors [7–9]. Woven column buckling behaviors, however, are more complicated due to local interactions between weavers (Fig. 1c). Recent work on woven materials has focused on implementing finite element analysis techniques [10–13] and semi-analytical modeling [14–16] to determine mechanical properties such as stiffness and buckling behaviors. These models require large computational power, and unlike an analytical model, they can only provide limited insight on the underlying mechanics of the system behavior. Moreover, the mechanical behavior of the cylindrical woven column unit has remained unexplored.

In this work, we derive purely analytical models for the stiffness and buckling forces of woven columns. Through physical experiments we explore the axial behavior of the column and verify the analytical models. We then classify global and local buckling modes of woven columns, and determine relationships between the buckling mode and the width of weavers. Our models and findings explain scaling laws where the stiffness and buckling load of woven columns change with the thickness and width of weavers. This work provides tools for choosing suitable weaver parameters for 3D woven column structures when they are to be designed for various potential engineering applications.

2. Mechanical model derivation

We use fundamental mechanics theory to derive models for the stiffness and critical buckling loads of a thin-walled, tightly woven column. These models are based on geometric parameters and material properties of the vertical and horizontal weavers we use to fabricate the columns.

2.1. Buckling of woven columns

We model the horizontal and vertical weavers in parallel, as shown in Fig. 2a. We assume that there is no nonlinear mechanical coupling, such as friction, between the weavers. Therefore, the vertical and horizontal weavers both behave linearly according to the physics

* Correspondence to: Deployable and Reconfigurable Structures Laboratory, Department of Civil and Environmental Engineering, University of Michigan, Ann Arbor, 48109, MI, USA.
E-mail address: filipov@umich.edu (E.T. Filipov).

https://doi.org/10.1016/j.mechrescom.2026.104702
Received 30 November 2025; Received in revised form 27 March 2026; Accepted 12 April 2026
Available online 23 April 2026

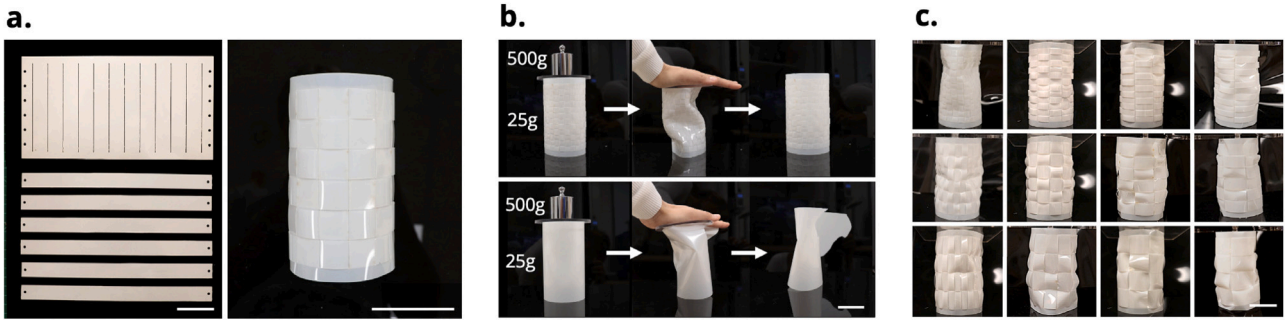

Fig. 1. Overview of the woven columns and their buckling behaviors which are explored in this work. a. Fabrication of a plain woven column, which is a fundamental unit for 3D woven shell structures. We assemble the vertical and horizontal weavers (left) into a woven column (right) using a plain weave pattern. b. A comparison shows that a woven column (top) does not experience permanent damage after buckling, whereas a continuous column (bottom) made with the same amount of material experiences plastic deformation and fracture. c. Buckling modes of twelve different woven columns, where localized out-of-plane deformations of weavers contribute to buckling of the columns. The buckling pattern is dependent on the parameters of the vertical and horizontal weavers. Scale bars are 5 cm.

defined in our model. By linear superposition, the critical buckling load of a woven column is the sum of the critical load of its vertical weavers and that of its horizontal weavers: $P_{cr,\ total} = P_{cr,\ h} + P_{cr,\ v}$. We first consider the critical load of vertical weavers $P_{cr,\ v}$. To simplify our model, we assume that the adjacent vertical weavers in a woven column initially buckle independently. Furthermore, by assuming a tightly woven cylinder, each segment of a vertical weaver along its length also behaves independently. Illustrated in Fig. 2c, the buckling force of a vertical weaver is then governed by the buckling force of a singular segment of length w_h. The load on a weaver with a small initial out-of-plane displacement can be approximated by the buckling force of an initially straight weaver since this force is minimally greater. Based on the Euler buckling theory, $P_{cr,\ v}$ is dependent on the width of vertical weavers w_v, the thickness of vertical weavers t_v, and the width of horizontal weavers w_h (which is also the length of each segment of a vertical weaver) [17]:

$$P_{cr,\ v} = n_v \frac{\pi^2 E \cdot w_v t_v^3}{w_h^2}, \tag{1}$$

where n_v is the total number of vertical weavers and E is the Young's modulus of the material.

Next, we consider the critical buckling load of the horizontal weavers $P_{cr,\ h}$. These weavers are assumed to be short cylindrical shells with axisymmetric sinusoidal initial perturbations. Based on previous research on thin-walled cylinders [7], the critical buckling load of a horizontal weaver is dependent on its normalized thickness t_h/R (where t_h is the thickness of horizontal weavers and R is the radius of the woven column) and the surface area of the horizontal weaver A_f. We use Koiter's knockdown factor β to account for the influence of the initial sinusoidal perturbation on the buckling load [8]:

$$P_{cr,\ h} = \beta \cdot \frac{E(t_h/R)}{\sqrt{3(1-\nu^2)}} \cdot A_f, \tag{2}$$

where ν is the Poisson's ratio. Axisymmetric sinusoidal perturbations greatly reduce the buckling force compared to a perfect cylindrical shell. To account for this influence, Koiter's knockdown factor β is solved implicitly using material parameters and the imperfection perturbation size δ_h shown in Fig. 2c [8,18]:

$$\beta \cdot \left(\frac{\delta_h}{t_h}\right) = \left(\frac{4}{27}(1-\nu^2)\right)^{1/2}(1-\beta)^2. \tag{3}$$

The perturbation term δ_h in Eq. (3) is calculated by approximating the horizontal weaver as a polygonal section with n_v sides where the length of each side is w_v. Then δ_h is the average distance of this polygon from a circle of equal circumference. Equivalently, we take half the distance between its maximum and minimum radii as in Fig. 2c to calculate the δ_h:

$$\delta_h = \frac{1}{2}\left(\frac{w_v}{2\sin(\frac{\pi}{n_v})} + \frac{w_v}{2\tan(\frac{\pi}{n_v})}\right). \tag{4}$$

We compute the buckling force of the horizontal weavers using Eqs. (2), (3), and (4). We then add it to the buckling force of the vertical weavers Eq. (1) to obtain the buckling force of the entire woven column.

2.2. Stiffness of woven columns

We model the vertical and horizontal weavers as springs in parallel with stiffnesses k_v and k_h (Fig. 2a). As in our critical force model, we assume that there is no nonlinear mechanical coupling, such as friction, between the weavers. Then, the vertical and horizontal weavers both behave linearly according to the physics defined in our model. We can then assume that the stiffness of a woven column is the sum: $k_{total} = k_h + k_v$. We first consider the vertical weaver stiffness k_v. We assume that the vertical weavers deform sinusoidally as they are compressed, and that bending deformations store significantly more energy than axial deformations. All vertical weavers act in parallel and resist bending deformations. The slender vertical weavers mainly bend about the favored axis of bending (the horizontal axis), but they also bend about the less favored axis of bending (the vertical axis). Therefore, the vertical weavers take on a curved cross-section due to the nature of weaving, and this pre-curvature increases their stiffness significantly by a factor α [19–21]. We balance forces and moments at the location of the greatest perturbation (as in Fig. 2c) to obtain a dependence of the axial load of the weaver P_v on flexural rigidity EI, number of vertical weavers n_v, out-of-plane curvature of the weaver κ, and linear displacement perturbation δ_v. Note that κ and δ_v are both functions of the axial displacement Δ. We calculate the stiffness as the derivative of axial load with respect to axial displacement:

$$k_v = \alpha \cdot \frac{n_v}{n_h} \cdot \frac{d}{d\Delta}\left(EI\frac{\kappa(\Delta)}{\delta_v(\Delta)}\right) \tag{5}$$

The factor α accounts for the significant effect of curvature induced stiffness [19–21], which increases with vertical weaver width. We apply Pini's equation [19] to the vertical weaver segments, using the radius of the woven column R, curvature of the vertical weavers κ, and Poisson's ratio ν:

$$\alpha = \frac{w_v^4}{60t_v^2}\left(\kappa - \frac{\nu}{R}\right)^2 + 1 \tag{6}$$

We assume that the out-of-plane displacement δ_v is small and that each vertical weaver deforms sinusoidally with n_h half-waves. We determine the maximum curvature κ of the vertical weavers using the

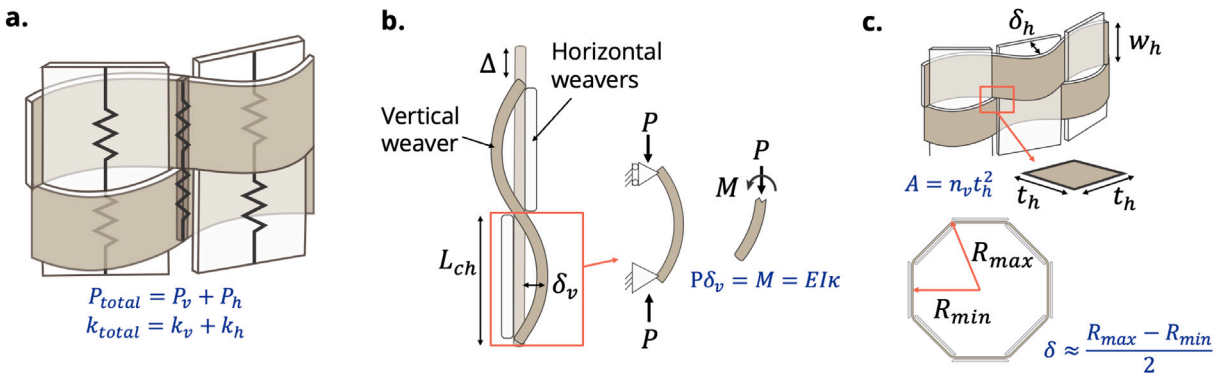

Fig. 2. Derivation of the stiffness and the buckling load of a woven column. a. Schematic of the horizontal and vertical weavers as vertical springs in parallel, and individual units as vertical springs in series. b. Schematic of the vertical weavers. Each segment of a vertical weaver is modeled as an independent column undergoing buckling. To derive stiffness, the inner force and bending moment are analyzed at locations of maximum curvature. c. Schematic of the horizontal weavers. Horizontal weavers are modeled as axisymmetric sinusoidally perturbed cylindrical shells stacked on top of one another. The horizontal cross-section is approximated as a polygon with n_v sides. Given a cross-section, the perturbation δ_h is derived by averaging R_{max} and R_{min}. The contact area A for deriving the horizontal stiffness is taken as the total contact area between adjacent horizontal weavers.

curvature formula [22], with the vertical weaver length being $n_h w_h$. At the location where the maximum curvature occurs, the curvature reduces to

$$\kappa = \delta_v \left(\frac{n_h \pi}{n_h w_h - \Delta} \right)^2. \tag{7}$$

Because $\kappa \propto \delta_v$ in Eq. (7), the derivative in Eq. (5) simplifies without further calculation of δ_v. Furthermore, we substitute $I = \frac{1}{12} w_v t_v^3$, $R = \frac{n_v w_v}{2\pi}$, and combine Eqs. (5), (6), and (7) into Eq. (8), which can be approximately described by the relationship $k_v \propto \frac{n_v w_v^5 t_v}{n_h^2 w_h^3}$.

$$k_v = \frac{E}{6} \frac{n_v w_v t_v^3 n_h \pi^2}{(n_h w_h - \Delta)^3} \cdot \underbrace{\left(\frac{w_v^4}{60 t_v^2} \left(\delta_v \left(\frac{n_h \pi}{n_h w_h - \Delta} \right)^2 - \frac{2\pi\nu}{n_v w_v} \right)^2 + 1 \right)}_{\text{Correction factor } \alpha}. \tag{8}$$

Horizontal weavers are modeled in series with one another with axial deformation in response to loading. The contact area $A = n_v t_h^2$ is the area between vertical weavers where adjacent horizontal weavers make contact, as shown in Fig. 2c. Thus, the contribution of the horizontal weavers to stiffness is

$$k_h = \frac{E n_v t_h^2}{n_h w_h}. \tag{9}$$

We sum Eqs. (8) and (9) to obtain the overall stiffness of a woven column.

3. Fabrication and experimental methods

We conducted a parametric study and validated our models through experimentation on woven cylindrical column samples. We constructed samples varying: (1) vertical weaver thickness t_v, (2) horizontal weaver thickness t_h, (3) vertical weaver width w_v, (4) horizontal weaver width w_h, and (5) sample height h. We construct a base woven column with $t_v = t_h = 0.191$ mm, $w_v = w_h = 20$ mm, and $h = 140$ mm. We then conduct five experiments, each keeping one parameter constant and varying the other four (Table 1). The sample height h is varied by changing the number of horizontal weavers n_h without changing any other parameters.

Our samples are woven by hand from vertical and horizontal strips of Mylar® polyester connected by a vertical seam of split pins (Fig. 3a). For studies with consistent vertical weaver thickness, we cut the vertical weavers from a continuous Mylar® sheet and leave a 10 mm connection at the top and bottom (Fig. 3a). This connection at the two ends assists fabrication and facilitates consistency in spacing, but may cause varying end effects when the vertical weaver thickness varies. In our parametric study where the thickness of vertical weavers varies, we instead connect vertical weavers using two additional rows of split pins (Fig. 3b). We maintain consistent tightness of the weaving across all samples by scaling the spacing between weavers proportionally to the thickness of the weavers, as outlined in Table 1.

Table 1
Woven column parameters for parametric studies on t_v, t_h, w_v, w_h, and n_h. Weaver spacing parameters d_v and d_h are chosen based on respective weaver thicknesses t_v and t_h.

t_v [mm]	t_h [mm]	w_v [mm]	w_h [mm]	n_h	d_v [mm]	d_h [mm]
0.191	0.191	10	20	6	0.100	0.100
0.191	0.191	12	20	6	0.100	0.100
0.191	0.191	15	20	6	0.100	0.100
0.191	0.191	20	20	6	0.100	0.100
0.191	0.191	24	20	6	0.100	0.100
0.191	0.191	30	20	6	0.100	0.100
0.191	0.191	40	20	6	0.100	0.100
0.191	0.191	20	10	6	0.100	0.100
0.191	0.191	20	12	6	0.100	0.100
0.191	0.191	20	15	6	0.100	0.100
0.191	0.191	20	24	6	0.100	0.100
0.191	0.191	20	30	6	0.100	0.100
0.191	0.191	20	40	6	0.100	0.100
0.102	0.191	20	20	6	0.053	0.100
0.254	0.191	20	20	6	0.133	0.100
0.356	0.191	20	20	6	0.186	0.100
0.191	0.102	20	20	6	0.100	0.053
0.191	0.254	20	20	6	0.100	0.100
0.191	0.356	20	20	6	0.100	0.186
0.191	0.191	20	20	3	0.100	0.100
0.191	0.191	20	20	9	0.100	0.100
0.191	0.191	20	20	12	0.100	0.100

We obtained the experimental buckling force, stiffness, and qualitative buckling mode for each woven sample using plate-to-plate compression loading between two acrylic plates (Fig. 3b, c, and d). The samples were compressed at a rate of 15 mm/min using a Mark-10® ESM 1500 single-column tabletop testing system with a 250 N load cell. Force and displacement are recorded at a sampling rate of 20 Hz until a global maximum force is reached. To account for precision error in sample fabrication, we tested three identical samples of each variation and calculated the average values and error ranges.

We observed that many of the columns exhibit a behavior in which smaller peaks, which we will later define as "local buckling", are reached before buckling. Due to this, the average slope before buckling is an underestimate for the stiffness of these columns. We choose buckling force as the peak load experienced, and stiffness as the maximum instantaneous slope before buckling (Fig. 3e). This instantaneous

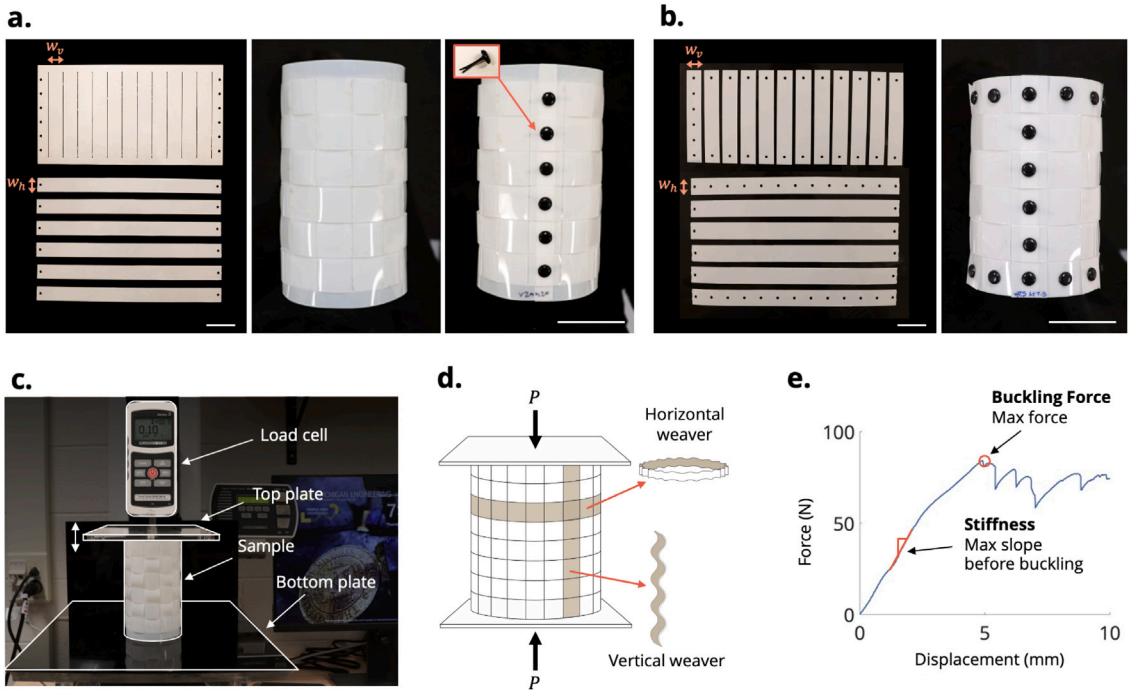

Fig. 3. Fabrication of woven columns and the test setup. a. Assembly of a column where vertical weavers are connected at the top and bottom. This design maintains consistent spacing in samples, but can only be used for testing in which the thickness of vertical weavers remains constant. Scale bars are 4 cm. b. Assembly of a column where vertical weavers are mechanically joined using split pins at the top and bottom of horizontal weavers. This design maintains consistent end effects, and is only used in a few of our tests where vertical thickness varies. Scale bars are 4 cm. c. Test setup using Mark-10® ESM 1500 single-column tabletop testing system. d. Schematic for plate-to-plate compression loading of woven columns. Vertical and horizontal weavers are both assumed to be deformed with sinusoidal deflections. e. A typical force–displacement curve obtained from an experiment with the buckling force and stiffness measured.

maximum stiffness most accurately captures the stiffness between local buckling events while also being able to capture an approximate average when there are no local buckling events. We applied a linear fit over every 1 mm displacement range of the data and identified the range with the maximum slope, which we defined as the stiffness. The displacement range of 1 mm was chosen because it is large enough to eliminate noise within small displacements, and it is small enough to accurately capture peak stiffness. We visually confirmed all stiffness calculations by plotting a short line at the location of the maximum stiffness and validating the selected range (Fig. 3e).

4. Results

Based on our parametric studies, we observed and classified the different buckling modes of woven columns. We compared our mechanical models for the buckling force and stiffness of woven columns to experimental data.

4.1. Buckling mode classification

In our parametric study, we vary the widths of vertical and horizontal weavers. We observed a strong correlation of buckling behavior with the weaver widths (Fig. 4a). We define the buckling behavior of a column as local if it experiences any local maxima in its force–displacement curve before 95% of the buckling force is reached. We define these local maxima as force values in which all forces within a ±0.4 mm displacement range are less than 93% of the local maximum value (Fig. 4c). We define the buckling behavior of the column as global if it does not exhibit these local maxima before peak buckling is reached (Fig. 4b). By using this criterion to distinguish local and global buckling modes, we find that for w_v much larger than w_h, local buckling is more often experienced. For w_h much larger than w_v, global buckling is more often experienced. Based on our experiment, the boundary between these two regions is dependent on both w_v and w_h.

We observed that the post buckling shape of a column is correlated with whether it buckles globally or locally. For the columns that experience the global buckling mode, under large deformations the horizontal and vertical weavers tend to deform together, typically into a diamond pattern (Fig. 4b). Even for this global buckling scenario, we believe that local buckling of vertical and horizontal weavers remains the precipitating factor, consistent with our assumptions in Section 2. For local buckling modes, initial buckling occurs in multiple locations before the system reaches a peak load (Fig. 4c). At the failure of a structure undergoing local buckling, these segments fail simultaneously, consistent with our assumptions in Section 2. We observe more global buckling in columns with wider horizontal weavers and narrower vertical weavers because these patterns allow the cylinder to buckle between horizontal boundaries. Meanwhile, when vertical weavers are wider and horizontal weavers are narrower, the curvature-stiffening effects of the vertical weavers counteracts buckling across horizontal boundaries, which results in more complicated local behaviors in post buckling behavior.

For columns experiencing global buckling, the force–displacement behavior before peak load is more predictable than for locally buckling columns. Therefore, applications requiring repeatable or predictable deformation such as in buckling-enabled soft robotics or mechanical computing may benefit from woven structures that undergo a global buckling mode. Our results suggest that the desired buckling modes for 3D woven structure can be specifically designed by adjusting the widths of the vertical and horizontal weavers.

4.2. Scaling relationships of buckling load

The buckling force of a woven column increases with both the thicknesses of its vertical and horizontal weavers, as validated in Fig. 5a and b. In our model, buckling force increases proportionally to the thickness of vertical weavers cubed ($P_{cr} \propto t_v^3$), resulting from the

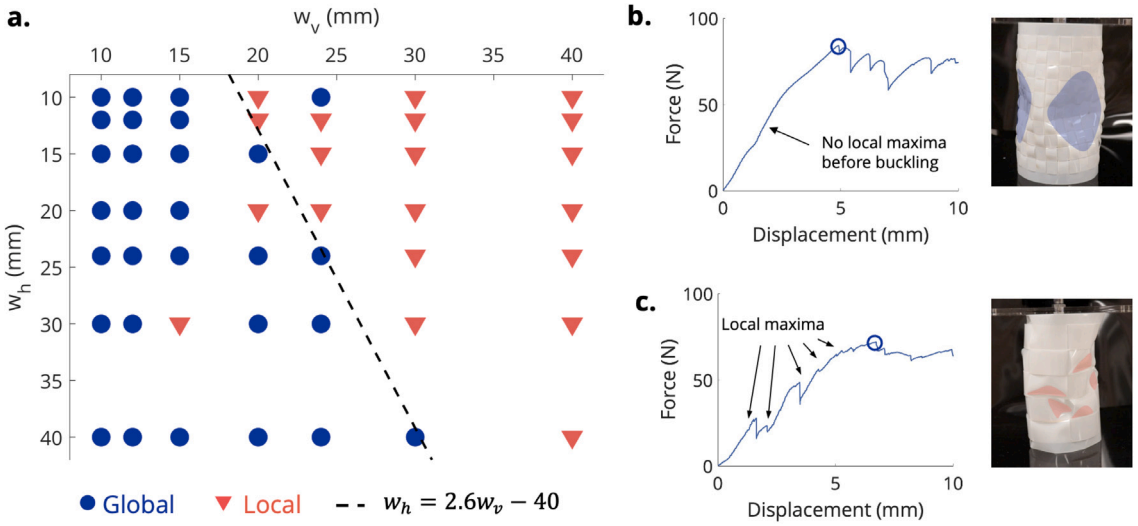

Fig. 4. Comparison of buckling modes. a. Depending on the widths of horizontal and vertical weavers in a woven column, the buckling mode of the column switches between global and local modes. A preliminary division between global and local modes is also approximated linearly. b. Typical force–displacement curve for a column that experiences global buckling into a diamond pattern, with no pre-buckling behavior observed. c. Typical force–displacement curve for a column that experiences local buckling, where pre-buckling is observed, and local force maxima occur before a peak force is obtained.

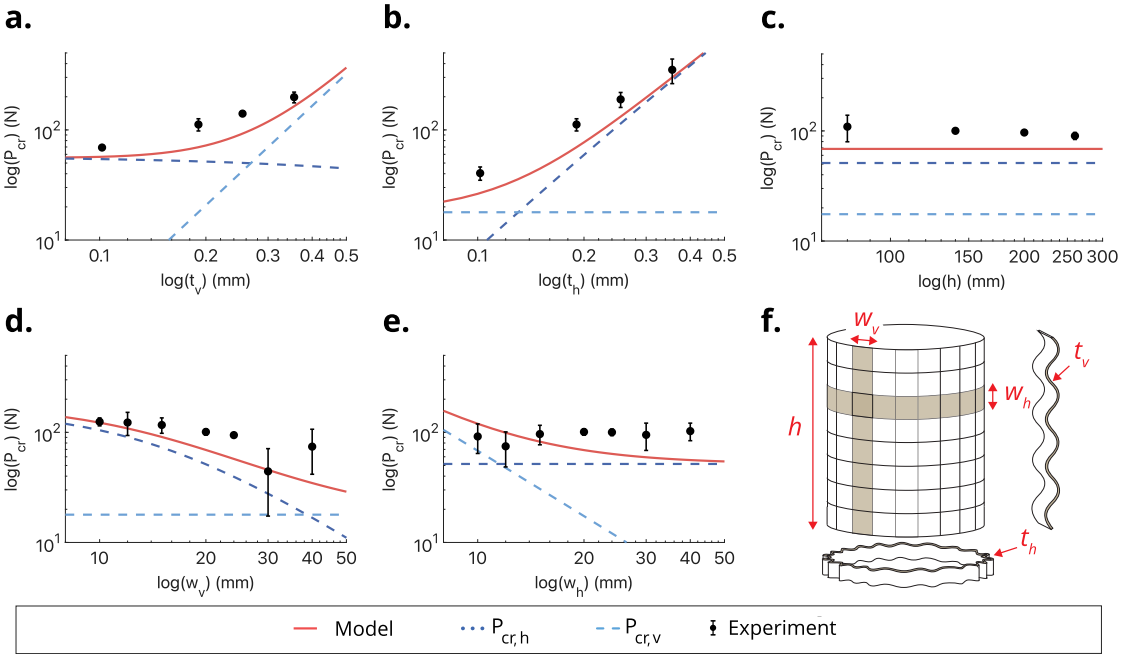

Fig. 5. Log–log scale: Influence of design parameters on buckling forces of woven columns. Buckling force with respect to: a. Vertical weaver thickness, b. Horizontal weaver thickness, c. Column height, d. Vertical weaver width, e. Horizontal weaver width. f. Schematic of all design parameters.

relationship of vertical weaver buckling force to the second moment of inertia (Fig. 5a). By comparing our experimental results on a log–log scale, we observe that the cubed factor may be larger than the true factor (Fig. 5a). The error in our buckling force model with respect to our horizontal thickness experiment is 30%, with the main source of error being from this factor (Table 2). Buckling force increases with the thickness of horizontal weavers as a result of the horizontal weaver buckling force component (Fig. 5b). Based on comparisons to our experimental data, our model underestimates $P_{cr,h}$, but its the vertical weaver buckling force component matches the trend of the data. The error in our buckling force model with respect to our horizontal thickness experiment is 30%, with the main source of error being from this underestimation (Table 2).

Shown in Fig. 5d and e, our buckling force model is compared to experimental data varying the widths of vertical and horizontal weavers. Increases in the width of vertical weavers w_v cause greater initial sinusoidal imperfections in horizontal weavers, making the horizontal weavers and the entire column more prone to buckling (Fig. 5d). By comparing our model, we see that our vertical weaver buckling force component decreases at a larger rate than in reality. The error in our buckling force model with respect to our horizontal thickness experiment is 23%, with the main source of error being from this discrepancy (Table 2). When the width of horizontal weavers w_h is varied, our idealized model predicts that for small widths of horizontal weavers, the vertical weavers will experience higher-order sinusoidal wave patterns and higher buckling forces (Fig. 5e). In reality, inconsistencies in weaving allow for weak spots where the vertical weavers form uneven

waves and the resulting buckling force is lower than predicted. These defects become more likely when horizontal weavers are less wide and vertical weavers have more segmental waves, so a realistically fabricated column will not experience substantial increases in buckling forces as the horizontal weaver widths become small (Fig. 5e). This effect on buckling force is most apparent in our data when horizontal and vertical widths are both less than 15 mm. In contrast, when the width of horizontal weavers w_h increases, the vertical weavers have few segmental waves and the buckling force approaches $P_{cr,h}$. Our model underestimates the value of $P_{cr,h}$, but it accurately captures the approach to a constant value for large w_h (Fig. 5e). The error in our buckling force model with respect to our horizontal width experiment is 33%, with the main source of error being from this underestimation (Table 2).

When considering the column height, there is a negligible effect on the buckling force compared to other parameters (Fig. 5c). Our model, similar to classical models for cylindrical shell buckling [8], does not account for the height of the column, so it matches this trend well. This result further supports our initial assumption, where local buckling of the vertical and horizontal weavers, rather than global system buckling, drive the behavior of the system. The error in our buckling force model with respect to our horizontal width experiment is 30%. We believe the main source of error is from underestimating the horizontal buckling force because we know that this quantity is underestimated based on our horizontal width and thickness experiments (Table 2).

4.3. Scaling relationships of stiffness

The stiffness of the woven column increases with respect to both its vertical and horizontal weaver thicknesses, as validated in Fig. 6a and b. By increasing vertical weaver thickness t_v, we increase the bending modulus of the vertical weavers by a factor of thickness cubed t_v^3, resulting in a stiffer structure (Fig. 6a). The error in our buckling force model with respect to our vertical thickness experiment is 5%, and we believe that our model accurately captures the effect of this parameter (Table 2). Our model predicts that we increase the horizontal weaver stiffness proportionally to their thickness squared ($k_h \propto t_h^2$) because the contact area between adjacent horizontal weavers increases with the thickness squared (Fig. 6b). This trend agrees with experimental data, with a relative error of 16% (Table 2).

Shown in Fig. 6d and e, our stiffness model is compared to experimental data varying vertical and horizontal weaver width. As the vertical weaver width w_v increases, the vertical weavers exhibit more curvature about the less favored vertical axis of bending, resulting in additional curvature-induced stiffness from the vertical weavers (Fig. 6d). As w_v decreases, the contact area between horizontal weavers increases, resulting in increased stiffness due to the horizontal weaver component of stiffness. Based on our direct comparison and in Fig. 6d and log–log comparison in Fig. 6d, we believe that our model may overestimate the effects of w_v smaller or larger than in the tested range. The model matches the data with a relative error of 16%, with the primary source of error being from an overestimation when compared against the smallest and largest tested widths (Table 2). As the horizontal weaver width w_h decreases, the vertical weavers have smaller periods with greater curvature relative to displacement, and thus higher stiffness (6e). As best seen in log–log scale, our model overestimates the power of w_h which $\frac{1}{k_v}$ is proportional to, which causes a great overestimate of k for small w_h. Additionally, it may be the case that k increases for large w_h rather than approaching k_h. We believe this could be due to effects such as friction losses between the horizontal weavers during loading, which we assume to be negligible in our model. The error in our stiffness model with respect to the horizontal width experiment is 65%, which the primary source being the overestimate for small w_h. When taken only based on $w_h > 12$, the relative error decreases to 28% (Table 2).

Table 2
Buckling force model error relative to data from each parametric study.

Parameter	t_v	t_h	h	w_v	w_h
Error in buckling force model (%)	15	30	30	23	33
Error in stiffness model (%)	5	16	36	16	65

When considering the height of the columns in Fig. 6c, the stiffness increases for shorter columns due to the contribution of the horizontal weavers. The stiffness increases exponentially for shorter columns because when keeping w_h constant, we have $h \propto n_h$ hence the relationship follows from $k_h \propto \frac{1}{n_h}$. Shown in our log–log comparison in Fig. 6c, our model overestimates the power in which k_h is proportional to $\frac{1}{h}$, which is the primary source of the 36% error in Table 2.

5. Discussions

5.1. Evaluation of analytical model

The purpose of our analytical model is to address the dominant physics of the buckling of woven columns. The model matches overall buckling and stiffness trends, supporting our mechanics theory. Limitations of our simplified approach are reflected in the relative errors presented in Table 2. These errors demonstrate that while our model addresses dominant physics, is not suitable for determining exact buckling load and stiffness quantities given a weave design.

We observe that our critical force model underestimates the buckling load (Fig. 5). The buckling knockdown factor we use in our derivation for $P_{cr,h}$ in Eqs. (2) and (3) corresponds with axisymmetric sinusoidal imperfections, making it the "worst case scenario" reduction. Since we are using this formula on short cylindrical columns with a length–radius ratio $L/R < 1.5$, our predictions are expected to underestimate the actual buckling load [8,18].

Additionally, our model accounts for the axial curvature effects of vertical weavers in predicting stiffness (Eq. (6)), but not directly when predicting buckling load. We believe that curvature greatly affects stiffness, and may also affect buckling load. We note from our results on buckling mode that local buckling occurs in columns composed of vertical weavers with greater curvature induced-stiffening relative to their characteristic length (larger vertical weaver width, smaller horizontal weaver width). Local buckling directly causes a reduction of curvature induced-stiffening, forcing weavers to buckle more closely to the sinusoidal shape assumed by our model. Because of this local buckling, the model is still predicting reasonable trends when vertical weavers are wider and local buckling occurs. However, since the shape of the vertical weavers is not perfectly sinusoidal in these cases, the model may be less accurate when curvature-induced stiffening and local buckling occur. This effect could explain the larger error for $w_v = 40$ in Fig. 5d.

Our model relies on the assumption of linearity in order to add horizontal and vertical weaver effects for buckling force and stiffness. Due to this assumption, our model is limited to weaver materials with low friction which do not exhibit nonlinear mechanical coupling between weavers. We validated our model using Mylar, which has a coefficient of friction of 0.5. We do not believe that our model would produce accurate results for materials with much higher coefficients of friction, as these materials may exhibit more nonlinear weaver–weaver interactions.

5.2. Evaluation of experimental data

We are able to use our experiment to evaluate multiple assumptions of our analytical model. We are able to visually identify that the vertical weavers deform in an approximately sinusoidal shape leading to buckling, which is a key assumption in our models for both

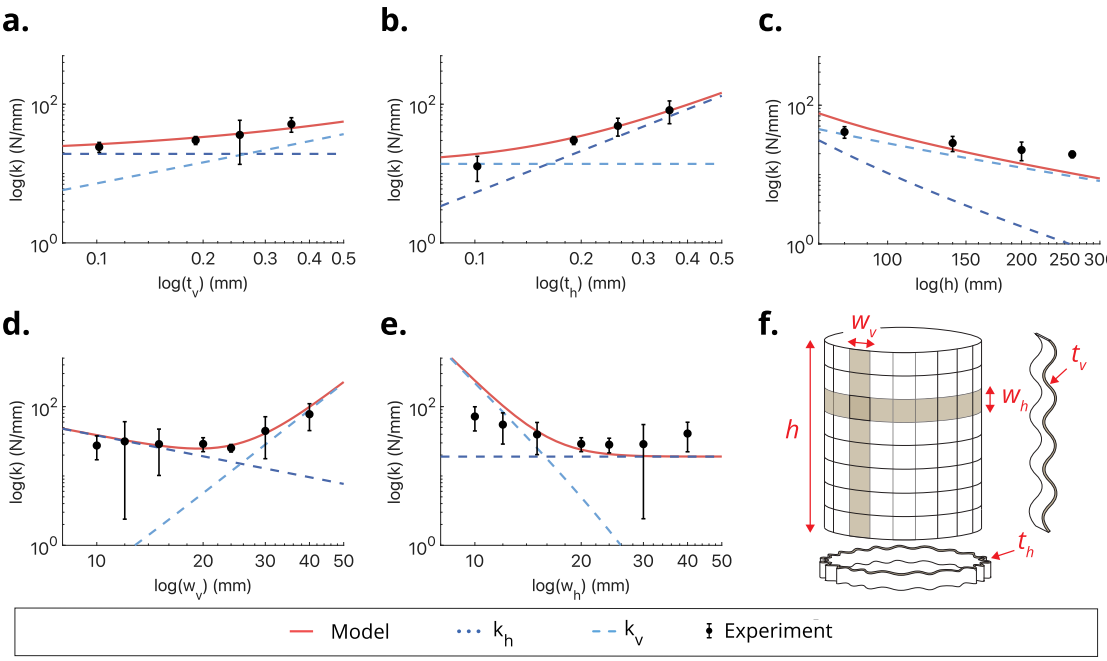

Fig. 6. Log–log scale: Influence of design parameters on the stiffness of woven columns. Stiffness with respect to: a. Vertical weaver thickness, b. Horizontal weaver thickness, c. Column height, d. Vertical weaver width, e. Horizontal weaver width. f. Schematic of all design parameters.

buckling force and stiffness. We observed slipping between vertical weavers when w_h is small, which causes weak spots resulting in a lower experimental critical force and stiffness. This differs from our model assumption that tight weaving results in independence between vertical weavers, and causes our model to be less reliable for small w_h. Our experiments support our assumption that vertical and horizontal weavers can be approximately modeled in parallel when there is low friction between weavers, as adding the respective critical force and stiffness components results in trends similar to the experimental data.

We observe much larger relative error within our experimental data regarding stiffness than for buckling force. We believe that the magnitude of these error bars is due to differences in the amounts of prebuckling experienced throughout the column. In the ideal scenario, every weaver experiences prebuckling by the same amount before buckling. In reality, some weavers remain straight for a longer period of time than others before buckling. This difference greatly impacts the standard deviation between stiffness calculations of different samples, resulting in very high error.

5.3. Next steps

Our initial study on buckling modes serves as a baseline for future work, in which the transition between buckling modes will be statistically analyzed and quantified using full-field finite-element simulations. Additionally, this future study can be used to quantify whether other parameters such as weaver thickness play a role in buckling mode behavior.

6. Conclusions

We created analytical models that predict the buckling force and stiffness of cylindrical woven columns made from a tight planar weave. The models are based on the geometry of the columns and basic mechanics principles, which makes the models versatile and simple to use. The models have been validated with experimental data considering different parameters, including weaver widths, weaver thicknesses, and column height. Our models explain the underlying mechanics behind buckling force and stiffness trends in woven structures and serve as a closed-form tool for design. We determined that while both vertical and horizontal weavers contribute to the overall column buckling force and stiffness, in some cases one or the other will have a larger influence on tuning a specific property. When thickness of either horizontal or vertical weavers is increased, both the buckling capacity and the stiffness increase. When we increase the width of horizontal weavers, the buckling capacity remains constant and the stiffness decreases. When we increase the width of vertical weavers, the buckling capacity decreases while the stiffness increases. Our results can inform design for efficient material use by identifying which weaver parameters can be changed to achieve a desired structural property.

We established predictive guidelines for the buckling mode of a column. We categorized a column's buckling mode as local if the column experiences local maxima in its force–displacement curve before buckling. A column's buckling mode is categorized as global if the column does not experience local maxima before buckling. These modes are largely dependent on horizontal and vertical weaver widths, and the transition between modes can be described by a relationship between horizontal and vertical weaver widths. Our initial experiment demonstrates that columns with larger vertical weaver widths and smaller horizontal weaver widths typically experience local buckling. Columns with smaller vertical weaver widths and larger horizontal weaver widths typically experience global buckling where the structure deforms into a diamond pattern.

Our findings serve to guide the design of woven structures such that favorable behaviors and buckling modes can be achieved, and buckling load and stiffness can be analytically calculated. These hierarchical woven structures have potential for future engineering applications in soft intelligent robots, flexible metamaterials, customizable wearable devices, and more.

CRediT authorship contribution statement

Jaimie Krankel: Writing – review & editing, Writing – original draft, Validation, Software, Methodology, Investigation, Formal analysis. **Guowei Wayne Tu:** Writing – review & editing, Supervision, Project administration, Methodology, Conceptualization. **Evgueni T. Filipov:** Writing – review & editing, Supervision, Funding acquisition, Conceptualization.

Declaration of competing interest

The authors declare that they have no known competing financial interests or personal relationships that could have appeared to influence the work reported in this paper.

Acknowledgments

The authors acknowledge support from the Air Force Office of Scientific Research, United States under award number FA9550-22-1-0321 and support from the University of Michigan Summer Undergraduate Research in Engineering (SURE) program. The paper reflects the views and opinions of the authors, and not necessarily those of the funding entities.

Data availability

Data will be made available on request.

References

[1] G.W. Tu, E.T. Filipov, Corner topology makes woven baskets into stiff, yet resilient metamaterials, Phys. Rev. Res. 7 (3) (2025) 033193, http://dx.doi.org/10.1103/9srl-9gsc.
[2] G.W. Tu, E.T. Filipov, Engineering snags for spatial curvature in weaves: fabrication, mechanics, and inverse design, Soft Matter 21 (2025) 8793–8802, http://dx.doi.org/10.1039/D5SM00813A.
[3] G.W. Tu, E.T. Filipov, Origami of multi-layered spaced sheets, J. Mech. Phys. Solids 190 (2024) 105730, http://dx.doi.org/10.1016/j.jmps.2024.105730.
[4] K. Jing, S. Xie, Y. Zhang, H. Zhou, H. Yan, Impact resistance of 3D woven fabrics and composites: A review, Thin-Walled Struct. 213 (2025) 113262, http://dx.doi.org/10.1016/j.tws.2025.113262.
[5] Z. Wang, A. Sobey, Many-objective design optimisation of a plain weave fabric composite, Compos. Struct. 285 (2022) 115246, http://dx.doi.org/10.1016/j.compstruct.2022.115246.
[6] I.A. Abu Bakar, O. Kramer, S. Bordas, T. Rabczuk, Optimization of elastic properties and weaving patterns of woven composites, Compos. Struct. 100 (2013) 575–591, http://dx.doi.org/10.1016/j.compstruct.2012.12.043.
[7] M.W. Hilburger, Buckling of Thin-Walled Circular Cylinders, NASA Special Publication NASA SP-8007-2020/REV 2, NASA, Hampton, VA, 2020, Revised version of NASA SP-8007 (1965).
[8] S. Gerasimidis, E. Virot, J.W. Hutchinson, S.M. Rubinstein, On establishing buckling knockdowns for imperfection-sensitive shell structures, J. Appl. Mech. 85 (9) (2018) http://dx.doi.org/10.1115/1.4040455.
[9] H. Ma, P. Jiao, H. Li, Z. Cheng, Z. Chen, Buckling analyses of thin-walled cylindrical shells subjected to multi-region localized axial compression: Experimental and numerical study, Thin-Walled Struct. 183 (2023) 110330, http://dx.doi.org/10.1016/j.tws.2022.110330.
[10] A.A. Kumar, A.K. Hii, S.R. Hallett, B.E. Said, Modelling woven composites with shell elements: An application of second-order computational homogenisation, Comput. Struct. 312 (2025) 107736, http://dx.doi.org/10.1016/j.compstruc.2025.107736.
[11] C.J.F. Júnior, V. Nandurdikar, A.G. Neto, A.B. Harish, Concurrent multiscale modelling of woven fabrics: Using beam finite elements with contact at mesoscale, Finite Elem. Anal. Des. 242 (2024) 104274, http://dx.doi.org/10.1016/j.finel.2024.104274.
[12] G. Nilakantan, M. Keefe, T.A. Bogetti, R. Adkinson, J.W. Gillespie, On the finite element analysis of woven fabric impact using multiscale modeling techniques, Int. J. Solids Struct. 47 (17) (2010) 2300–2315, http://dx.doi.org/10.1016/j.ijsolstr.2010.04.029.
[13] Q.T. Nguyen, T.D. Nguyen, D.V. Dao, D.V. Le, T.T. Nguyen, A study on mechanical properties of 3D printing ABS plastic according to different printing orientations, IOP Conf. Ser.: Mater. Sci. Eng. 459 (1) (2018) http://dx.doi.org/10.1088/1757-899X/459/1/012082.
[14] D. Luo, Y. Zhong, S. Xi, Z. Shi, Static, buckling, and free-vibration analysis of plain-woven composite plate with finite thickness using VAM-based equivalent model, Thin-Walled Struct. 169 (2021) 108503, http://dx.doi.org/10.1016/j.tws.2021.108503.
[15] H. Dabiryan, M. Jesri, H.R. Ovesy, Z.S. Mazloomi, Numerical and experimental study of buckling behavior of delaminated plate in glass woven fabric composite laminates, J. Eng. Fibers Fabr. 17 (2022) http://dx.doi.org/10.1177/15589250221091268.
[16] M. El Messiry, S. El-Tarfawy, Mechanical properties and buckling analysis of woven fabric, Text. Res. J. 89 (14) (2018) 2900–2918, http://dx.doi.org/10.1177/0040517518803777.
[17] R. Hibbeler, Mechanics of Materials, Pearson, 2015.
[18] W. Koiter, The effect of axisymmetric imperfections on the buckling of cylindrical shells under axial compression, Proc. K. Ned. Akad. Wet. B 66 (5) (1963) 265–279.
[19] V. Pini, J. Ruz, P. Kosaka, P. Maletinsky, C. Meyer, M. Esashi, R.H. Blick, How two-dimensional bending can extraordinarily stiffen thin sheets, Sci. Rep. 6 (2016) 29627, http://dx.doi.org/10.1038/srep29627.
[20] M. Taffetani, F. Box, A. Neveu, D. Vella, Limitations of curvature-induced rigidity: How a curved strip buckles under gravity, Europhys. Lett. 127 (1) (2019) 14001, http://dx.doi.org/10.1209/0295-5075/127/14001.
[21] T. Barois, L. Tadrist, C. Quilliet, Y. Forterre, How a curved elastic strip opens, Phys. Rev. Lett. 113 (2014) 214301, http://dx.doi.org/10.1103/PhysRevLett.113.214301.
[22] S.J. Colley, Vector Calculus, fifth ed., Pearson, Boston, 2018.